PERGAMON

International Journal of Solids and Structures 39 (2002) 3893–3906

INTERNATIONAL JOURNAL OF SOLIDS and STRUCTURES

www.elsevier.com/locate/ijsolstr

The elastic modulus of single-wall carbon nanotubes: a continuum analysis incorporating interatomic potentials

P. Zhang [a], Y. Huang [a,*], P.H. Geubelle [b], P.A. Klein [c], K.C. Hwang [d]

[a] *Department of Mechanical and Industrial Engineering, University of Illinois at Urbana-Champaign, 1206 West Green Street, Urbana, IL 61801, USA*

[b] *Department of Aeronautical and Astronautical Engineering, University of Illinois, Urbana, IL 61801, USA*

[c] *Sandia National Laboratories, Livermore, CA 94551, USA*

[d] *Department of Engineering Mechanics, Tsinghua University, Beijing 100084, China*

Received 13 February 2002

Abstract

A nanoscale continuum theory is established to directly incorporate interatomic potentials into a continuum analysis without any parameter fitting. The theory links interatomic potentials and atomic structure of a material to a constitutive model on the continuum level. The theory is applied to study the linear elastic modulus of a single-wall carbon nanotube. The Young's modulus predicted by this nanoscale continuum theory agrees well with prior experimental results and atomistic studies. © 2002 Elsevier Science Ltd. All rights reserved.

Keywords: Elastic modulus; Carbon nanotube; Continuum analysis; Interatomic potential

1. Introduction

Interest in carbon nanotubes continues to grow since their first discovery (Iijima, 1991; Ebbesen and Ajayan, 1992) and the establishment of new effective methods to produce them (Thess et al., 1996). Carbon nanotubes are cylinders of graphene with diameters from 1 to 2 nm. They have single or multiple layers of carbon atoms in the tube thickness direction, and are called single-wall carbon nanotubes (SWNTs) and multi-wall carbon nanotubes (MWNTs), respectively. Carbon nanotubes have the potential to be the interconnects in molecular electronics, or to be transistors that are 500 times smaller than current devices. Both MWNTs and SWNTs in bundles are complex conductors that incorporate many coupled tubes/shells that each of which possesses either metallic (m) or semiconducting (s) electronic structures. Although s-nanotubes can be switched on and off as field-effect transistors, no method exists yet to selectively prepare or separate s-nanotubes from m-nanotubes. This has been seen as the primary hurdle to nanotube-based electronics (see MRS Bulletin 26 (2001) 495–497). The recent work of Collins et al. (2001) provided a novel

* Corresponding author. Fax: +1-217-244-6534.
E-mail address: huang9@uiuc.edu (Y. Huang).

PII: S0020-7683(02)00186-5

technique to convert MWNTs into either metallic or semiconducting conductors and to fabricate arrays of field-effect transistors from SWNTs. This represents a major step to overcome the hurdle to nanotube-based electronics.

Carbon nanotubes display unique coupling between the electrical properties and mechanical deformation. Tombler et al. (2000) used the tip of an atomic force microscope/microscopy (AFM) to deflect a suspended SWNT with both ends clamped to metal electrodes. They observed that the electrical conductivity of an SWNT is reduced by two orders of magnitude upon deformation; i.e., the electrical conductivity of an undeformed, metal-like SWNT decreases by nearly 100 times after the AFM tip deforms the carbon nanotube. Moreover, this transformation is completely reversible since there is no change in the electrical conductivity upon complete unloading of the AFM. This unique behavior makes carbon nanotubes an ideal candidate for nanoscale sensors and nano-electro-mechanical systems (NEMS).

Carbon nanotubes also display superior mechanical properties and may be used as potential reinforcements in nanocomposite materials and many other applications (Ruoff and Lorents, 1995; Govindjee and Sackman, 1999; Srivastava et al., 2001; Yakobson and Avouris, 2001). The deformation of an SWNT is completely reversible (i.e., elastic) subjected to strains of more than 4% (Iijima et al., 1996; Falvo et al., 1997; Wong et al., 1997; Hertel et al., 1998; Lourie et al., 1998; Wagner et al., 1998; Walters et al., 1999; Tombler et al., 2000; Yu et al., 2000a). A 6-nm long SWNT with 1-nm diameter may sustain a large compressive strain of 5% prior to buckling, and even larger strains under torsion (Yakobson et al., 1996). Experimental investigations (e.g., Yu et al., 2000b) and atomistic studies (Yakobson et al., 1997) on fracture of SWNTs and MWNTs showed that carbon nanotubes can sustain strains larger than 10% prior to fracture.

There are some experimental studies of the elastic modulus of carbon nanotubes. Treacy et al. (1996) obtained the Young's moduli of carbon nanotubes from transmission electron microscopy (TEM) observations of the thermal vibration of an MWNT. A large variation of Young's moduli was reported, from 0.40 to 4.15 TPa with an average of 1.8 TPa. Krishnan et al. (1998) also used TEM to observe the thermal vibration of an SWNT at room temperature and reported Young's moduli of SWNTs in the range from 0.90 to 1.70 TPa, with an average of 1.25 TPa. Wong et al. (1997), Salvetat et al. (1999) and Tombler et al. (2000) used AFM to bend an MWNT, nanoropes of SWNTs and a single SWNT, respectively. A large variation of Young's modulus was also reported for MWNTs (0.69–1.87 TPa) by Wong et al. (1997), while the Young's modulus was 0.6 TPa for nanoropes of SWNTs (Salvetat et al., 1999) and 1.2 TPa for SWNTs (Tombler et al., 2000). Yu et al. (2001a,b) conducted nanoscale tensile tests of an MWNT pulled by AFM tips under a scanning electron microscope. The Young's moduli of MWNTs ranged from 0.27 to 0.95 TPa. The scanning force microscopy characterization of individual carbon nanotubes on electrode arrays under bending gave the Young's modulus of MWNTs as 1 TPa (Muster et al., 1998), while the micro-Raman spectroscopy study of carbon nanotubes under cooling-induced compression provided an estimate of the Young's modulus from 2.8 to 3.6 TPa for SWNTs, and 1.7 to 2.4 TPa for MWNTs (Lourie and Wagner, 1998). Contrary to these microscopy studies, Pan et al. (1999) measured directly the Young's modulus from the tensile tests of ropes of very long and aligned MWNTs, and reported much lower Young's moduli from 0.22 to 0.68 TPa.

There are also extensive atomistic studies to investigate the Young's modulus of carbon nanotubes. Robertson et al. (1992) used the molecular dynamics with the interatomic potential for carbon (Tersoff, 1988; Brenner, 1990) and local density functional to study an SWNT and reported a Young's modulus around 1.02 TPa. The interatomic potential of Tersoff (1988) and Brenner (1990) has also been used in other molecular dynamics studies of SWNTs, and a large variation of Young's moduli has been reported (e.g., 1.07 TPa by Yakobson et al. (1996); 0.8 TPa by Cornwell and Wille (1997); 0.44–0.50 TPa by Halicioglu (1998)). There are also molecular dynamics studies using other interatomic potentials, such as the Keating potential, summation of pairwise harmonic potentials, and the potential accounting for both bond stretching and bond angle changes adopted by Overney et al. (1993), Lu (1997) and Prylutskyy et al. (2000),

respectively. The corresponding Young's modulus is 1.5 TPa (Overney et al., 1993), 0.97 TPa (Lu, 1997), and 1.1–1.2 TPa (Prylutskyy et al., 2000). Lu (1997) also obtained slightly larger Young's moduli (0.97–1.11 TPa) for MWNTs as compared to his SWNT results. Popov et al. (2000) determined the Young's modulus of SWNTs to be 1 TPa from the analytical expressions for the elastic modulus for SWNTs which they obtained using Born and Huang's (1954) perturbation technique for a lattice–dynamical model of nanotubes (Popov et al., 1999). Similar to the large variations of Young's moduli obtained from molecular dynamics simulations, the tight-binding methods also give large scattering in Young's modulus of an SWNT, ranging from 0.67 TPa (Molina et al., 1996) to 1.26 TPa (Hernández et al., 1998, 1999; Goze et al., 1999; Vaccarini et al., 2000). There are also first-principles calculations of the elastic modulus of SWNTs, which once again give significant variations in results. Sánchez-Portal et al.'s (1999) study based on pseudopotential density functional theory gave Young's moduli from 0.95 to 1.10 TPa, while Van Lier et al.'s (2000) ab initio multiplicative integral approach yielded Young's moduli ranging from 0.75 to 1.18 TPa. Recently, Zhou et al.'s (2001) first-principles study based on linear combination of atomic orbitals and molecular orbital cluster determined the Young's modulus of an SWNT to be 0.76 TPa.

There are, however, very few continuum studies of carbon nanotubes because it is generally thought that continuum mechanics theories are not applicable on the atomic or nanometer scale. Among these limited continuum studies, a carbon nanotube is either modeled as a cylindrical shell (e.g., Yakobson et al., 1996; Ru, 2000a,b, 2001), a beam (Liu et al., 2001), or many truss members (Odegard et al., 2001). Two critical parameters in the shell model, namely the elastic modulus and shell thickness of a carbon nanotube, are determined by fitting the tensile and bending stiffness obtained from molecular dynamics simulations (Yakobson et al., 1996). The corresponding buckling strain and buckling mode predicted by the linear elastic shell model for the same carbon nanotube under compression then agree reasonably well with molecular dynamics simulations (Iijima et al., 1996; Yakobson et al., 1996).

For potential applications of carbon nanotubes in nanoelectronics, NEMS, and nanocomposite materials, it is desirable to have nanoscale continuum theories that may overcome some limitations of the atomistic studies concerning both time scales (10^{-12}–10^{-9} s) and length scales (10^{-9}–10^{-6} m). Moreover, the future success of nanotechnology requires the development of nanoscale continuum theories that are directly linked to atomistic models or atomistic simulations. Tadmor et al. (1996a,b) and co-workers (Miller et al., 1998a,b; Shenoy et al., 1998, 1999) proposed a quasi-continuum model to link atomistic simulation with continuum analysis, where the atomistic simulation was applied over regions of relatively nonuniform deformation while the continuum analysis was used over domains of uniform deformation. Friesecke and James (1999) proposed an approach to pass the atomistic information to a continuum theory for a nanostructure in which one or more dimensions are large relative to atomic scale. Gao et al. (2001) studied dynamic fracture at the nanometer scale via both molecular dynamics simulations and continuum mechanics analysis. Without any parameter fitting, the continuum mechanics analysis agreed very well with the molecular dynamics simulation even down to a few atomic spacings. This suggests that, under certain conditions, the continuum mechanics theories are applicable on the nanometer scale.

Zhang et al. (2002a) proposed a nanoscale continuum theory that directly incorporates the interatomic potential into the constitutive model of the solid. A systematic approach was adopted to derive the continuum strain energy density from the energy stored in the atomic bonds by averaging over the bond orientations and distribution. Such an approach involves no parameter fitting and leads naturally to a continuum constitutive model for nanostructured materials. Based on the interatomic potentials for carbon (Tersoff, 1988; Brenner, 1990), Zhang et al. (2002a) applied this nanoscale continuum theory to carbon nanotubes and studied the instability of an SWNT under uniaxial tension. Two approximations were made to simplify the theory: (i) the interaction between the atoms was considered only via the pair potential, i.e., the multi-body coupling with the local environment was neglected; and (ii) the bond density function was uniform, which gave an isotropic constitutive model within the tube surface. This nanoscale continuum theory predicted a bifurcation strain of 52% that, without any parameter fitting, agreed well with the critical

strain of 55% at the onset of instability of a carbon nanotube observed in molecular dynamics simulations (Yakobson et al., 1997) using the same interatomic potential.

The purpose of the present study is to generalize Zhang et al.'s (2002a) nanoscale continuum theory without making the above two assumptions of pair-potential-only interaction and uniform bond density function. The interaction between a pair of carbon atoms depends not only on the stretched bond length, but also on the local environment (i.e., atoms outside the pair), as characterized by the Tersoff's (1988) and Brenner's (1990) interatomic potential summarized in Section 2. A nanoscale continuum theory for carbon nanotubes is established in Section 3 for the noncentrosymmetric, hexagonal lattice structure of graphite and carbon nanotube. The elastic modulus of carbon nanotubes are obtained in Section 4, and are compared with the aformentioned experimental data and atomistic simulations.

2. Interatomic potential for carbon

Tersoff (1988) and Brenner (1990) determined the interatomic potential for carbon as

$$V(r_{ij}) = V_{\mathrm{R}}(r_{ij}) - B_{ij}V_{\mathrm{A}}(r_{ij}), \tag{1}$$

for atoms i and j, where r_{ij} is the distance between atoms i and j, V_{R} and V_{A} are the repulsive and attractive pair terms given by

$$V_{\mathrm{R}}(r) = \frac{D^{(e)}}{S-1}\mathrm{e}^{-\sqrt{2S}\beta(r-R^{(e)})}f_{\mathrm{c}}(r), \tag{2}$$

$$V_{\mathrm{A}}(r) = \frac{D^{(e)}S}{S-1}\mathrm{e}^{-\sqrt{2/S}\beta(r-R^{(e)})}f_{\mathrm{c}}(r), \tag{3}$$

the parameters $D^{(e)}$, S, β, and $R^{(e)}$ are determined from the known physical properties of carbon, graphite and diamond, and are given at the end of this section; the function f_{c} is merely a smooth cutoff function to limit the range of the potential, and is given by

$$f_{\mathrm{c}}(r) = \begin{cases} 1 & r < R^{(1)}, \\ \frac{1}{2}\left\{1 + \cos\left[\frac{\pi(r-R^{(1)})}{R^{(2)}-R^{(1)}}\right]\right\} & R^{(1)} < r < R^{(2)}, \\ 0 & r > R^{(2)}, \end{cases} \tag{4}$$

which is continuous and has a cutoff of $R^{(2)} = 0.2$ nm and $R^{(1)} = 0.17$ nm to include only the first-neighbor shell for carbon.

The parameter B_{ij} in (1) represents a multi-body coupling between the bond from atom i to atom j and the local environment of atom i, and is given by

$$B_{ij} = \left[1 + \sum_{k\,(\neq i,j)} G(\theta_{ijk})f_{\mathrm{c}}(r_{ik})\right]^{-\delta}, \tag{5}$$

where r_{ik} is the distance between atoms i and k, f_{c} is the cutoff function in (4), θ_{ijk} is the angle between bonds i–j and i–k, and the function G is given by

$$G(\theta) = a_0\left[1 + \frac{c_0^2}{d_0^2} - \frac{c_0^2}{d_0^2 + (1+\cos\theta)^2}\right]. \tag{6}$$

For atoms i and j having different local environment, Brenner (1990) suggested to replace the coefficient B_{ij} in (5) by

$$\overline{B}_{ij} = (B_{ij} + B_{ji})/2. \tag{7}$$

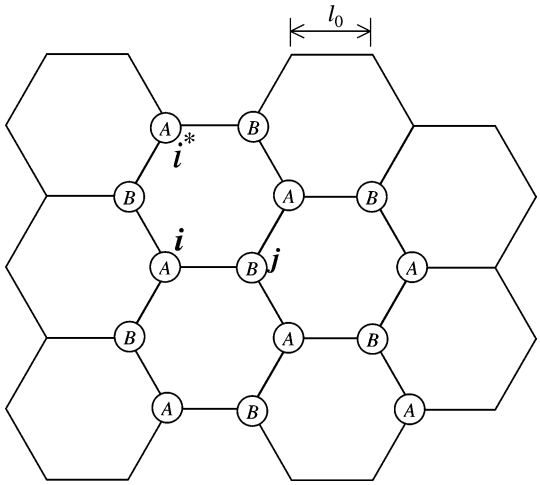

Fig. 1. A schematic diagram of the atomic structure of a graphite or carbon nanotube within the tube surface.

The parameters $D^{(e)}$, S, β and $R^{(e)}$ in (2) and (3), δ in (5), and a_0, c_0 and d_0 in (6) have been determined by Brenner (1990) to fit the binding energy and lattice constants of graphite, diamond, simple cubic and face-centered-cubic structures for pure carbon, as well as the vacancy formation energy for diamond and graphite. In fact, Brenner (1990) gave two sets of parameters for carbon,

$$\begin{aligned} &\text{(I)}\quad D^{(e)} = 6.325\ \text{eV}, \quad S = 1.29, \quad \beta = 15\ \text{nm}^{-1}, \quad R^{(e)} = 0.1315\ \text{nm};\\ &\qquad \delta = 0.80469;\\ &\qquad a_0 = 0.011304, \quad c_0 = 19, \quad d_0 = 2.5; \end{aligned} \tag{8}$$

and

$$\begin{aligned} &\text{(II)}\quad D^{(e)} = 6.000\ \text{eV}, \quad S = 1.22, \quad \beta = 21\ \text{nm}^{-1}, \quad R^{(e)} = 0.1390\ \text{nm};\\ &\qquad \delta = 0.50000;\\ &\qquad a_0 = 0.00020813, \quad c_0 = 330, \quad d_0 = 3.5. \end{aligned} \tag{9}$$

An SWNT has a hexagonal atomic structure within the tube surface, as shown in Fig. 1. The equilibrium bond length, denoted by l_0, is determined by minimizing the interatomic potential, or equivalently, by enforcing the force to vanish in each atomic bond i–j,

$$\frac{\partial V}{\partial r_{ij}} = 0. \tag{10}$$

This gives the equilibrium bond length as $l_0 = 0.142$ and 0.145 nm for the two sets of parameters (8) and (9), respectively. Both results agree reasonably well with the well-known bond length of graphite (0.144 nm).

3. A nanoscale continuum theory for materials with noncentrosymmetric atomic structure

Fig. 2 shows a schematic diagram of the multi-scale approach adopted by Zhang et al. (2002a) to establish a nanoscale continuum theory from the interatomic potential and the atomic structure of the material. Such an approach has also been used by Gao and Klein (1998), Klein and Gao (1998, 2000) and Zhang et al. (2002b) to incorporate an empirical cohesive force law into the constitutive model of solids. Each material point on the continuum level is surrounded by a small representative cell within which the

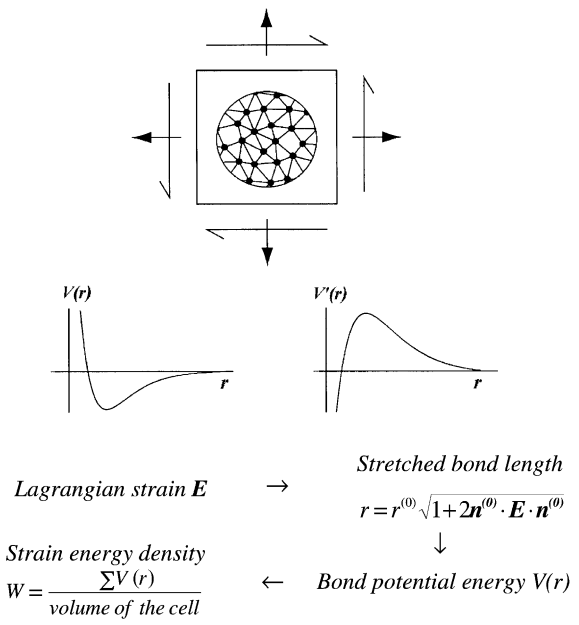

Fig. 2. A multi-scale framework to establish a nanoscale continuum theory from the interatomic potential and the atomic structure of the material.

deformation is uniform. The strain energy density on the continuum level is evaluated by the bond energy on the atomic level for all atomic bonds in the cell, i.e., by the so-called Cauchy–Born rule (e.g., Milstein, 1980; Tadmor et al., 1996a). This approach is first reviewed in the following for materials with centrosymmetric atomic structure and pair or multi-body interatomic potentials. It is then generalized for materials with noncentrosymmetric atomic structure (e.g., carbon nanotubes).

3.1. Materials with centrosymmetric atomic structure and pair interatomic potential

Let $\boldsymbol{E}$ denote the Lagrangian strain tensor on the continuum level, and $r_{ij}^{(0)}$ and $\boldsymbol{n}_{\boldsymbol{ij}}^{(\mathbf{0})}$ the unstretched bond length and unit vector in the initial bond orientation for atoms i and j at equilibrium, respectively. The stretched bond length after the strain $\boldsymbol{E}$ is imposed becomes

$$r_{ij} = r_{ij}^{(0)}\sqrt{1 + 2\boldsymbol{n}_{\boldsymbol{ij}}^{(\mathbf{0})}\cdot\boldsymbol{E}\cdot\boldsymbol{n}_{\boldsymbol{ij}}^{(\mathbf{0})}}. \tag{11}$$

The energy stored in the bond between atoms i and j is denoted by $V(r_{ij})$, where V is the pair interatomic potential. The strain energy stored in the representative cell is $\sum_{i<j} V(r_{ij})$, where the summation is over all atomic bonds within the cell. The strain energy density at this material point on the continuum level is then related to the interatomic potential V by

$$W = \frac{1/2\sum_{i,j} V(r_{ij})}{\Omega_\epsilon}, \tag{12}$$

where the factor 1/2 comes from the equal splic of bond energy to each atom, Ω_ϵ is the volume of the representative cell. The second (symmetric) Piola–Kirchhoff stress $\boldsymbol{T}$ is the work conjugate of the Lagrangian strain $\boldsymbol{E}$, and is obtained from (12) by

$$\boldsymbol{T} = \frac{\partial W}{\partial \boldsymbol{E}} = \frac{1}{2\Omega_\epsilon} \sum_{i,j} \frac{V'(r_{ij})}{r_{ij}} (r_{ij}^{(0)})^2 \boldsymbol{n}_{\boldsymbol{ij}}^{(\boldsymbol{0})} \boldsymbol{n}_{\boldsymbol{ij}}^{(\boldsymbol{0})}, \tag{13}$$

which is related to the Lagrangian strain $\boldsymbol{E}$ via the stretched bond length r_{ij} in (11).

3.2. Materials with centrosymmetric atomic structure and multi-body interatomic potential

It should be pointed out, however, that the energy stored in the bond between atoms i and j may also depend on the atoms outside the pair, i.e., it is described by a multi-body interatomic potential

$$V = V(r_{ij}; r_{ik}, \theta_{ijk}, k \neq i, j), \tag{14}$$

where k denotes all atoms outside the pair i–j, $r_{ik} = r_{ik}^{(0)}(1 + 2\boldsymbol{n}_{\boldsymbol{ik}}^{(\boldsymbol{0})} \cdot \boldsymbol{E} \cdot \boldsymbol{n}_{\boldsymbol{ik}}^{(\boldsymbol{0})})^{1/2}$ is the stretched bond length between atoms i and k; θ_{ijk} is the angle between deformed bonds i–j and i–k, and is given by

$$\cos\theta_{ijk} = \frac{r_{ij}^2 + r_{ik}^2 - r_{jk}^2}{2 r_{ij} r_{ik}}, \tag{15}$$

and $r_{jk} = r_{jk}^{(0)}(1 + 2\boldsymbol{n}_{\boldsymbol{jk}}^{(\boldsymbol{0})} \cdot \boldsymbol{E} \cdot \boldsymbol{n}_{\boldsymbol{jk}}^{(\boldsymbol{0})})^{1/2}$. An example of the multi-body interatomic potentials is given in (1) for carbon (Tersoff, 1988; Brenner, 1990), where the multi-body interaction comes into play via the coefficient B_{ij}. Zhang et al. (2002a) estimated B_{ij} to be 0.96 for a graphite structure or carbon nanotube, and therefore approximated it by unity such that the interatomic potential then became a pair potential, i.e., $V \approx V(r_{ij})$. Such an approximation is removed in the present analysis in order to accurately account for the multi-body interaction of carbon atoms in a nanotube. Accordingly, the strain energy density is given by

$$W = \frac{\sum_{i,j} V(r_{ij}; r_{ik}, \theta_{ijk}, k \neq i, j)}{2\Omega_\epsilon}, \tag{16}$$

and the second Piola–Kirchhoff stress becomes

$$\boldsymbol{T} = \frac{\partial W}{\partial \boldsymbol{E}} = \frac{1}{\Omega_\epsilon} \sum_{i<j} \left[\frac{\partial V}{\partial r_{ij}} \frac{(r_{ij}^{(0)})^2}{r_{ij}} \boldsymbol{n}_{\boldsymbol{ij}}^{(\boldsymbol{0})} \boldsymbol{n}_{\boldsymbol{ij}}^{(\boldsymbol{0})} + \sum_{k(\neq i,j)} \frac{\partial V}{\partial r_{ik}} \frac{(r_{ik}^{(0)})^2}{r_{ik}} \boldsymbol{n}_{\boldsymbol{ik}}^{(\boldsymbol{0})} \boldsymbol{n}_{\boldsymbol{ik}}^{(\boldsymbol{0})} + \sum_{k(\neq i,j)} \frac{\partial V}{\partial \theta_{ijk}} \frac{\partial \theta_{ijk}}{\partial \boldsymbol{E}} \right], \tag{17}$$

where $\partial\theta_{ijk}/\partial\boldsymbol{E}$ is obtained from (15).

3.3. Materials with noncentrosymmetric atomic structure

It must be pointed out that the Cauchy–Born rule linking the continuum strain energy density to the interatomic potential requires the atomic structure of the solid to have centrosymmetry. The graphite structure of a carbon nanotube clearly does not meet this requirement. Rigorously speaking, one cannot simply apply the Cauchy–Born rule to a carbon nanotube since a "homogeneously deformed" carbon nanotube on the representative cell level may undergo inhomogeneous deformation inside the cell. In fact, Klein (1999) showed that the inappropriate use of the Cauchy–Born rule for a material with noncentrosymmetric microstructure may lead to completely unphysical and incorrect results. In order to overcome this limitation, Zhang et al. (2002a) approximated the hexagonal graphite wall of a nanotube by a comparison medium having randomized bond structure but identical mass density and Young's modulus as the graphite. This was achieved by taking a uniform and isotropic bond density function such that the comparison medium has the centrosymmetry required by the Cauchy–Born rule. Such an approximation is removed in the present study of an SWNT, as discussed in the following.

Even though the hexagonal lattice of a graphite sheet does not possess centrosymmetry, it can be decomposed to two sub-lattices marked by A and B shown in Fig. 1, and each sub-lattice has a triangular

lattice structure and possesses centrosymmetry. Let $\boldsymbol{F}$ denote the uniform deformation gradient on the continuum level at an arbitrary point i in the sub-lattice A. Another arbitrary point i^* in the same sub-lattice A moves to $\boldsymbol{F}\cdot\boldsymbol{R}_{ii^*}^{(0)}$ after the deformation, where $\boldsymbol{R}_{ii^*}^{(0)}$ is the vector from points i to i^* in the initial, undeformed configuration. Besides being subjected to the same deformation gradient $\boldsymbol{F}$, the sub-lattice B may also undergo a rigid body translation with respect to the sub-lattice A. Without losing generality, this translation may be written as $\boldsymbol{F}\cdot\boldsymbol{\xi}$ such that any point j in the sub-lattice B moves to

$$\boldsymbol{F}\cdot\boldsymbol{R}_{ij}^{(0)}+\boldsymbol{F}\cdot\boldsymbol{\xi}=\boldsymbol{F}\cdot\left(\boldsymbol{R}_{ij}^{(0)}+\boldsymbol{\xi}\right), \tag{18}$$

after the deformation, where $\boldsymbol{R}_{ij}^{(0)}$ is the vector from points i to j in the initial, undeformed configuration, and the vector $\boldsymbol{\xi}$ is to be determined by the minimization of the strain energy density, as discussed later. The stretched length of bond i–j after the deformation then becomes

$$r_{ij}=\sqrt{\left(\boldsymbol{R}_{ij}^{(0)}+\boldsymbol{\xi}\right)\cdot\boldsymbol{F}^{\boldsymbol{T}}\cdot\boldsymbol{F}\cdot\left(\boldsymbol{R}_{ij}^{(0)}+\boldsymbol{\xi}\right)}=\sqrt{\left(\boldsymbol{R}_{ij}^{(0)}+\boldsymbol{\xi}\right)\cdot(\boldsymbol{I}+2\boldsymbol{E})\cdot\left(\boldsymbol{R}_{ij}^{(0)}+\boldsymbol{\xi}\right)}, \tag{19}$$

where the Lagrangian tensor $\boldsymbol{E}$ is related to the deformation gradient $\boldsymbol{F}$ by $\boldsymbol{E}=\frac{1}{2}\left(\boldsymbol{F}^{\boldsymbol{T}}\cdot\boldsymbol{F}-\boldsymbol{I}\right)$, and $\boldsymbol{I}$ is the second-order identity tensor.

The strain energy density W is related to the multi-body interatomic potential V via (16). For a graphite structure in Fig. 1, the representative cell surrounding each atom in the sub-lattice A includes only three neighboring atoms in the sub-lattice B such that the strain energy density W becomes

$$W=\frac{\sum_{1\leqslant j\leqslant 3}V(r_j;r_k,\theta_{jk},k\neq j)}{2\Omega_\epsilon}, \tag{20}$$

where the subscript i (as in (16)) has been omitted since there is only one (central) atom from sub-lattice A in the representative cell, V is the interatomic potential for carbon given in (1),

$$\Omega_\epsilon=\frac{3\sqrt{3}}{4}l_0^2, \tag{21}$$

l_0 is the unstretched bond length for a graphite structure at equilibrium and is given at the end of Section 2,

$$r_j=l_0\sqrt{\left(\boldsymbol{n}_{\boldsymbol{j}}^{(0)}+\boldsymbol{x}\right)\cdot(\boldsymbol{I}+2\boldsymbol{E})\cdot\left(\boldsymbol{n}_{\boldsymbol{j}}^{(0)}+\boldsymbol{x}\right)}, \tag{22}$$

$$r_k=l_0\sqrt{\left(\boldsymbol{n}_{\boldsymbol{k}}^{(0)}+\boldsymbol{x}\right)\cdot(\boldsymbol{I}+2\boldsymbol{E})\cdot\left(\boldsymbol{n}_{\boldsymbol{k}}^{(0)}+\boldsymbol{x}\right)}, \tag{23}$$

$$\cos\theta_{ijk}=\frac{r_j^2+r_k^2-r_{jk}^2}{2r_jr_k}, \tag{24}$$

$$r_{jk}=l_0\sqrt{\boldsymbol{n}_{\boldsymbol{jk}}^{(0)}\cdot(\boldsymbol{I}+2\boldsymbol{E})\cdot\boldsymbol{n}_{\boldsymbol{jk}}^{(0)}}, \tag{25}$$

$\boldsymbol{n}_{\boldsymbol{j}}^{(0)}$ and $\boldsymbol{n}_{\boldsymbol{k}}^{(0)}$ are the unit vectors from the central atom in the sub-lattice A to the neighboring atoms j and k in the sub-lattice B, and $\boldsymbol{x}=\boldsymbol{\xi}/l_0$ is the normalized vector of the rigid body translation between the two sub-lattices A and B. The atoms j and k are both within the sub-lattice B such that its stretched bond length r_{jk} does not involve the vector $\boldsymbol{x}$.

For a given deformation gradient $\boldsymbol{F}$ (or equivalently the Lagrangian strain $\boldsymbol{E}$), the vector $\boldsymbol{x}$ related to the rigid body translation between two sub-lattices A and B is determined by minimizing the strain energy density W with respect to $\boldsymbol{x}$, i.e.,

$$\frac{\partial W}{\partial \boldsymbol{x}} = 0, \tag{26}$$

which gives

$$\sum_{1 \leqslant j \leqslant 3} \left[\frac{\partial V}{\partial r_j} \frac{(\boldsymbol{I} + 2\boldsymbol{E}) \cdot \left(\boldsymbol{n}_j^{(0)} + \boldsymbol{x} \right)}{r_j} + \sum_{k \neq j} \frac{\partial V}{\partial r_k} \frac{(\boldsymbol{I} + 2\boldsymbol{E}) \cdot \left(\boldsymbol{n}_k^{(0)} + \boldsymbol{x} \right)}{r_k} + \sum_{k \neq j} \frac{\partial V}{\partial \theta_{jk}} \frac{\partial \theta_{jk}}{\partial \boldsymbol{x}} \right] = 0, \tag{27}$$

where $\partial \theta_{jk}/\partial \boldsymbol{x}$ is obtained from (24) (and $\partial r_{jk}/\partial \boldsymbol{x} = 0$). The above nonlinear equation needs to be solved numerically in order to determine $\boldsymbol{x}$ in terms of the Lagrangian strain $\boldsymbol{E}$, i.e., $\boldsymbol{x} = \boldsymbol{x}(\boldsymbol{E})$, and the strain energy density can then be written as $W = W[\boldsymbol{E}, \boldsymbol{x}(\boldsymbol{E})]$. It is straightforward to verify that $\boldsymbol{x} = \boldsymbol{0}$ once $\boldsymbol{E} = \boldsymbol{0}$ (i.e., no deformation).

The second Piola–Kirchhoff stress $\boldsymbol{T}$ is related to the Lagrangian strain $\boldsymbol{E}$ from the total derivative D of strain energy density W,

$$\boldsymbol{T} = \frac{\mathrm{D}W}{\mathrm{D}\boldsymbol{E}} = \frac{\partial W}{\partial \boldsymbol{E}} + \frac{\partial W}{\partial \boldsymbol{x}} \cdot \frac{\partial \boldsymbol{x}}{\partial \boldsymbol{E}} = \frac{\partial W}{\partial \boldsymbol{E}} = \frac{1}{2\Omega_\epsilon} \sum_{1 \leqslant j \leqslant 3} \left[\frac{\partial V}{\partial r_j} \frac{\partial r_j}{\partial \boldsymbol{E}} + \sum_{k \neq j} \frac{\partial V}{\partial r_k} \frac{\partial r_k}{\partial \boldsymbol{E}} + \sum_{k \neq j} \frac{\partial V}{\partial \theta_{jk}} \frac{\partial \theta_{jk}}{\partial \boldsymbol{E}} \right], \tag{28}$$

where the fact $\partial W/\partial \boldsymbol{x} = 0$ in (26) has been used, $\partial r_j/\partial \boldsymbol{E}$, $\partial r_k/\partial \boldsymbol{E}$ and $\partial \theta_{jk}/\partial \boldsymbol{E}$ are obtained from (22)–(24), respectively. For an arbitrary strain $\boldsymbol{E}$, the above equation gives the stress $\boldsymbol{T}$, i.e., it provides the constitutive law of SWNTs under mechanical deformation. The constitutive law, together with the equilibrium equation and boundary conditions, provide a nanoscale continuum theory incorporating interatomic potentials.

The stress increment $\dot{\boldsymbol{T}}$ is related to the strain increment $\dot{\boldsymbol{E}}$ via the incremental modulus tensor $\boldsymbol{C}$,

$$\dot{\boldsymbol{T}} = \boldsymbol{C} : \dot{\boldsymbol{E}}, \tag{29}$$

where

$$\boldsymbol{C} = \frac{\mathrm{D}\boldsymbol{T}}{\mathrm{D}\boldsymbol{E}} = \frac{\mathrm{D}}{\mathrm{D}\boldsymbol{E}} \left(\frac{\partial W}{\partial \boldsymbol{E}} \right) + \frac{\mathrm{D}}{\mathrm{D}\boldsymbol{E}} \left(\frac{\partial W}{\partial \boldsymbol{x}} \right) \cdot \frac{\partial \boldsymbol{x}}{\partial \boldsymbol{E}} + \frac{\partial W}{\partial \boldsymbol{x}} \cdot \frac{\mathrm{D}}{\mathrm{D}\boldsymbol{E}} \left(\frac{\partial \boldsymbol{x}}{\partial \boldsymbol{E}} \right). \tag{30}$$

The last two terms of the right-hand side of (30) vanish because of $\partial W/\partial \boldsymbol{x} = 0$ in (26) and its derivative $\mathrm{D}/\mathrm{D}\boldsymbol{E}(\partial W/\partial \boldsymbol{x}) = 0$. Therefore,

$$\boldsymbol{C} = \frac{\mathrm{D}}{\mathrm{D}\boldsymbol{E}} \left(\frac{\partial W}{\partial \boldsymbol{E}} \right) = \frac{\partial^2 W}{\partial \boldsymbol{E} \partial \boldsymbol{E}} + \frac{\partial^2 W}{\partial \boldsymbol{E} \partial \boldsymbol{x}} \cdot \frac{\partial \boldsymbol{x}}{\partial \boldsymbol{E}}, \tag{31}$$

where $\partial \boldsymbol{x}/\partial \boldsymbol{E}$ is obtained from the total derivative of $\partial W/\partial \boldsymbol{x} = 0$ in (26),

$$\frac{\partial^2 W}{\partial \boldsymbol{x} \partial \boldsymbol{E}} + \frac{\partial^2 W}{\partial \boldsymbol{x} \partial \boldsymbol{x}} \cdot \frac{\partial \boldsymbol{x}}{\partial \boldsymbol{E}} = 0. \tag{32}$$

Its substitution into (31) yields

$$\boldsymbol{C} = \frac{\partial^2 W}{\partial \boldsymbol{E} \partial \boldsymbol{E}} - \frac{\partial^2 W}{\partial \boldsymbol{E} \partial \boldsymbol{x}} \cdot \left(\frac{\partial^2 W}{\partial \boldsymbol{x} \partial \boldsymbol{x}} \right)^{-1} \cdot \frac{\partial^2 W}{\partial \boldsymbol{x} \partial \boldsymbol{E}}. \tag{33}$$

It can be verified that the stress and modulus established above in terms of the interatomic potential also hold if an atom in the sub-lattice B is taken as the central atom surrounded by three neighboring atoms in the sub-lattice A. This is because the local environment of atoms in the sub-lattices A and B are the same.

4. Elastic modulus of single-wall carbon nanotubes

A nonlinear nanoscale continuum theory incorporating interatomic potentials is established in the previous section. The linear elastic modulus of an SWNT can be obtained from this nonlinear continuum theory by taking a vanishing deformation in (33), $\boldsymbol{E} = \boldsymbol{0}$. It can be verified straightforwardly from (27) that, for $\boldsymbol{E} = \boldsymbol{0}$, the vector $\boldsymbol{x}$ corresponding to the rigid body translation between the two sub-lattices vanishes, $\boldsymbol{x} = \boldsymbol{0}$, and so does the second Piolo–Kirchhoff stress $\boldsymbol{T}$, $\boldsymbol{T} = \boldsymbol{0}$, determined from (27).

The linear elastic modulus tensor is obtained from (33) by

$$\boldsymbol{C} = \left[\frac{\partial^2 W}{\partial \boldsymbol{E} \partial \boldsymbol{E}} - \frac{\partial^2 W}{\partial \boldsymbol{E} \partial \boldsymbol{x}} \cdot \left(\frac{\partial^2 W}{\partial \boldsymbol{x} \partial \boldsymbol{x}} \right)^{-1} \cdot \frac{\partial^2 W}{\partial \boldsymbol{x} \partial \boldsymbol{E}} \right]_{\boldsymbol{E}=\boldsymbol{0}, \boldsymbol{x}=\boldsymbol{0}}. \tag{34}$$

The second-order derivatives of the strain energy density W on the right-hand side of (34) can be expressed in terms of the first- and second-order derivatives of the interatomic potential V in (1) as well as the first- and second-order derivatives of deformed bond lengths and angle r_j, r_k and θ_{jk} in (22)–(24). The lengthy and tedious expressions of the derivatives are not presented here except two first-order derivatives of the interatomic potential V,

$$\left(\frac{\partial V}{\partial r_j} \right)_{\boldsymbol{E}=\boldsymbol{0}, \boldsymbol{x}=\boldsymbol{0}} = 0, \quad \left(\frac{\partial V}{\partial r_k} \right)_{\boldsymbol{E}=\boldsymbol{0}, \boldsymbol{x}=\boldsymbol{0}} = 0. \tag{35}$$

Let Z denote the axial direction of an SWNT, and θ the circumferential direction. The nonvanishing components of the linear elastic modulus tensor in (34) are denoted by C_{ZZZZ}, $C_{\theta\theta\theta\theta}$ and $C_{ZZ\theta\theta} = C_{\theta\theta ZZ}$. For simple tension along the axial direction Z of the tube, the Young's modulus is given by

$$E = C_{ZZZZ} - \frac{C_{ZZ\theta\theta}^2}{C_{\theta\theta\theta\theta}}. \tag{36}$$

It does not depend on the chirality of a carbon nanotube (Saito et al., 1998) because three uniformly spaced atomic bonds attached to each atom give an isotropic linear elastic modulus tensor $\boldsymbol{C}$ within the tube surface. This is, in fact, consistent with the molecular dynamics simulations (e.g., Lu, 1997).

It should be pointed out, however, that the elastic modulus tensor $\boldsymbol{C}$ in (34) and Young's modulus E in (36) for an SWNT are actually the linear elastic tensile stiffness rather than the modulus, i.e., they are the modulus multiplied by the tube thickness. It can be verified that the dimensions of $\boldsymbol{C}$ and E are Newton/meter (rather than N/m^2). This is because, though the interatomic potential V has the dimension of energy (eV $= 1.6 \times 10^{-19}$ N m), the "volume" of the representative cell Ω_ϵ in (21) is in fact the average area (rather than volume) per atom. In other words, the strain energy density W in (20) is the strain energy per unit tube surface area of an SWNT.

We have calculated the linear elastic tensile stiffness in (36) along the axial direction of an SWNT for the two sets of parameters (8) and (9) of the interatomic potential of carbon (Brenner, 1990). The resulting tensile stiffness is 159 N/m for the first set of parameters (8), and 236 N/m for the second set (9). While these two sets of parameters give the same binding energy and lattice constants for carbon (e.g., graphite, diamond), it is a bit puzzling that they predict different tensile stiffness for an SWNT. Moreover, which one agrees better with the experimental data and with atomistic studies of SWNTs?

As Brenner (1990) pointed out, each set of parameters in the interatomic potential was determined by fitting the binding energy and lattice constants of graphite, diamond and other possible atomic structures of pure carbon. The binding energy is directly related to the interatomic potential, while the lattice constants are the bond length at equilibrium, which are directly linked to the first-order derivatives of the interatomic

potential. Little or essentially no attention was paid to the second-order derivatives of the interatomic potential, but these second-order derivatives are closely related to the elastic moduli of graphite and diamond. Therefore, for the same binding energy and lattice constants of carbon, different methods of fitting give different sets of parameters in the interatomic potential (Brenner, 1990), which lead to different predictions of the tensile stiffness as shown above.

The Young's modulus of an SWNT can be obtained from the linear elastic tensile stiffness in (36) divided by the nanotube thickness h. This is consistent with the molecular dynamics calculations of the Young's modulus (e.g., Yakobson et al., 1996; Yakobson and Avouris, 2001). A common estimate of the nanotube thickness is the monoatomic layer thickness $h = 0.335$ nm, though this estimate is more suitable for MWNTs than for SWNTs (Yakobson and Avouris, 2001). For the first set of parameters (8) of the interatomic potential for carbon, the Young's modulus is 159 N/m/0.335 nm = 475 GPa, which is lower than those reported in most experimental and atomistic studies of SWNTs, and agrees only with Halicioglu's (1998) molecular dynamics calculations. The Young's modulus calculated from the second set of parameters (9) of the interatomic potential for carbon is 236 N/m/0.335 nm = 705 GPa. This falls in the range of Young's modulus reported by most experimental and atomistic studies of SWNTs (e.g., Molina et al., 1996; Cornwell and Wille, 1997; Salvetat et al., 1999; Van Lier et al., 2000; Zhou et al., 2001), but is either higher or lower than other reported Young's modulus. In particular, it agrees well with the molecular dynamics calculations of Cornwell and Wille (1997) using the same interatomic potential (Tersoff, 1988; Brenner, 1990).

The Young's modulus of an SWNT calculated from the present nanoscale continuum theory based on the second set of parameters in (9) of the interatomic potential of carbon agrees reasonably well with the experimental and atomistic studies of SWNTs.

5. Concluding remarks

A nanoscale continuum theory has been established to directly incorporate the interatomic potential into the continuum analysis of the solids. Once the interatomic potential and the atomic structure of the material are known, a systematic approach, which does not involve any parameter fitting, has been proposed to link the constitutive model on the continuum level to the interatomic potential of the material with the centrosymmetric atomic structure. We have applied this nanoscale continuum theory to study the elastic modulus of an SWNT based on the interatomic potential of carbon (Tersoff, 1988; Brenner, 1990). The atomic structure of an SWNT, however, does not possess the centrosymmetry such that the above approach must be modified based on energy minimization. The linear elastic modulus of an SWNT predicted by the present nanoscale continuum theory based on the interatomic potential (1) and (9) for carbon (Brenner, 1990) agrees reasonably well with the available experimental and atomistic studies.

It should be pointed out that the present approach to establish a nanoscale continuum theory is not limited to SWNTs; it can also be applied to other nanostructured materials once the interatomic potential and the atomic structure of the material are known. In fact, the present approach is not limited to materials with known interatomic potentials since other atomistic studies that provide energy in atomic bonds can be similarly incorporated in the present nanoscale continuum theory.

Acknowledgements

Y.H. acknowledges the support from NSF (grant #CMS-0099909) and from the M&IE Program of Exploratory Studies at UIUC. K.C.H. acknowledges the support from the NSF of China.

References

Born, M., Huang, K., 1954. Dynamical theory of the crystal lattices. Oxford University Press, Oxford.

Brenner, D.W., 1990. Empirical potential for hydrocarbons for use in simulation the chemical vapor deposition of diamond films. Physical Review B 42, 9458–9471.

Collins, P.G., Arnold, M.S., Avouris, P., 2001. Engineering carbon nanotubes and nanotube circuits using electrical breakdown. Science 292, 706–709.

Cornwell, C.F., Wille, L.T., 1997. Elastic properties of single-walled carbon nanotubes in compression. Solid State Communications 101, 555–558.

Ebbesen, T.W., Ajayan, P.M., 1992. Large-scale synthesis of carbon nanotubes. Nature 358, 220–222.

Falvo, M.R., Clary, G.J., Taylor II, R.M., Chi, V., Brooks Jr., F.P., Washburn, S., Superfine, R., 1997. Bending and buckling of carbon nanotubes under large strain. Nature 389, 582–584.

Friesecke, G., James, R.D., 1999. A scheme for the passage from atomic to continuum theory for thin films, nanotubes and nanorods. Journal of the Mechanics and Physics of Solids 48, 1519–1540.

Gao, H., Huang, Y., Abharam, F.A., 2001. Continuum and atomistic studies of intersonic crack propagation. Journal of the Mechanics and Physics of Solids 49, 2113–2132.

Gao, H.J., Klein, P., 1998. Numerical simulation of crack growth in an isotropic solid with randomized internal cohesive bonds. Journal of the Mechanics and Physics of Solids 46, 187–218.

Govindjee, S., Sackman, J.L., 1999. On the use of continuum mechanics to estimate the properties of nanotubes. Solid State Communications 110, 227–230.

Goze, C., Vaccarini, L., Henrard, L., Bernier, P., Hernández, E., Rubio, A., 1999. Elastic and mechanical properties of carbon nanotubes. Synthetic Metals 103, 2500–2501.

Halicioglu, T., 1998. Stress calculations for carbon nanotubes. Thin Solid Films 312, 11–14.

Hernández, E., Goze, C., Bernier, P., Rubio, A., 1998. Elastic properties of C and $B_xC_yN_z$ composite nanotubes. Physical Review Letters 80, 4502–4505.

Hernández, E., Goze, C., Bernier, P., Rubio, A., 1999. Elastic properties of single-wall nanotubes. Applied Physics A: Materials Science and Processing 68, 287–292.

Hertel, T., Martel, R., Avouris, Ph., 1998. Manipulation of individual carbon nanotubes and their interaction with surfaces. Journal of Physical Chemistry B 102, 910–915.

Iijima, S., 1991. Helical microtubules of graphitic carbon. Nature 354, 56–58.

Iijima, S., Brabec, C., Maiti, A., Bernholc, J., 1996. Structural flexibility of carbon nanotubes. Journal of Chemical Physics 104, 2089–2092.

Klein, P.A., 1999. A virtual internal bond approach to modeling crack nucleation and growth. Ph.D. dissertation, Stanford University, Palo Alto, CA 94305.

Klein, P.A., Gao, H., 1998. Crack nucleation and growth as strain localization in a virtual-bond continuum. Engineering Fracture Mechanics 61, 21–48.

Klein, P.A., Gao, H., 2000. Study of crack dynamics using the virtual internal bond method. Multiscale deformation and fracture in materials and structures. In: James, R. (Ed.), Rice's 60th Anniversary Volume. Kluwer Academic Publishers, Dordrecht, The Netherlands, pp. 275–309.

Krishnan, A., Dujardin, E., Ebbesen, T.W., Yianilos, P.N., Treacy, M.M.J., 1998. Young's modulus of single-walled nanotubes. Physical Review B 58, 14013–14019.

Liu, J.Z., Zheng, Q., Jiang, Q., 2001. Effect of a rippling mode on resonances of carbon nanotubes. Physical Review Letters 86, 4843–4846.

Lourie, O., Cox, D.M., Wagner, H.D., 1998. Buckling and collapse of embedded carbon nanotubes. Physical Review Letters 81, 1638–1641.

Lourie, O., Wagner, H.D., 1998. Evaluation of Young's modulus of carbon nanotubes by micro-Raman spectroscopy. Journal of Materials Research 13, 2418–2422.

Lu, J.P., 1997. Elastic properties of carbon nanotubes and nanoropes. Physical Review Letters 79, 1297–1300.

Miller, R., Ortiz, M., Phillips, R., Shenoy, V., Tadmor, E.B., 1998a. Quasicontinuum models of fracture and plasticity. Engineering Fracture Mechanics 61, 427–444.

Miller, R., Tadmor, E.B., Phillips, R., Ortiz, M., 1998b. Quasicontinuum simulation of fracture at the atomic scale. Modelling and Simulation in Materials Science and Engineering 6, 607–638.

Milstein, F., 1980. Review: theoretical elastic behaviour at large strains. Journal of Material Science 15, 1071–1084.

Molina, J.M., Savinsky, S.S., Khokhriakov, N.V., 1996. A tight-binding model for calculations of structures and properties of graphitic nanotubes. Journal of Chemical Physics 104, 4652–4656.

Muster, J., Burghard, M., Roth, S., Duesberg, G.S., Hernández, E., Rubio, A., 1998. Scanning force microscopy characterization of individual carbon nanotubes on electrode arrays. Journal of Vacuum Science and Technology B 16, 2796–2801.

Odegard, G.M., Gates, T.S., Nicholson, L.M., Wise, K.E., 2001. Equivalent-continuum modeling of nano-structured materials. NASA Technical Report, NASA/TM-2001-210863.

Overney, G., Zhong, W., Tomanek, D., 1993. Structural rigidity and low-frequency vibrational modes of long carbon tubules. Zeitschrift für Physik D: Atoms, Molecues and Clusters 27, 93–96.

Pan, Z.W., Xie, S.S., Lu, L., Chang, B.H., Sun, L.F., Zhou, W.Y., Wang, G., Zhang, D.L., 1999. Tensile tests of ropes of very long aligned multiwall carbon nanotubes. Applied Physics Letters 74, 3152–3154.

Popov, V.N., Van Doren, V.E., Balkanski, M., 1999. Lattice dynamics of single-walled carbon nanotubes. Physical Review B 59, 8355–8358.

Popov, V.N., Van Doren, V.E., Balkanski, M., 2000. Elastic properties of single-walled carbon nanotubes. Physical Review B 61, 3078–3084.

Prylutskyy, Y.I., Durov, S.S., Ogloblya, O.V., Buzaneva, E.V., Scharff, P., 2000. Molecular dynamics simulation of mechanical, vibrational and electronic properties of carbon nanotubes. Computational Materials Science 17, 352–355.

Robertson, D.H., Brenner, D.W., Mintmire, J.W., 1992. Energetics of nanoscale graphitic tubules. Physical Review B 45, 12592–12595.

Ru, C.Q., 2000a. Effective bending stiffness of carbon nanotubes. Physical Review B 62, 9973–9976.

Ru, C.Q., 2000b. Elastic buckling of single-walled carbon nanotube ropes under high pressure. Physical Review B 62, 10405–10408.

Ru, C.Q., 2001. Axially compressed buckling of a doublewalled carbon nanotube embedded in an elastic medium. Journal of the Mechanics and Physics of Solids 49, 1265–1279.

Ruoff, R.S., Lorents, D.C., 1995. Mechanical and thermal properties of carbon nanotubes. Carbon 33, 925–930.

Saito, R., Dresselhaus, G., Dresselhaus, M.S., 1998. Physical properties of carbon nanotubes. Imperial College Press, London.

Salvetat, J.P., Briggs, G.A.D., Bonard, J.M., Bacsa, R.R., Kulik, A.J., Stöckli, T., Burnham, N.A., Forró, L., 1999. Elastic and shear moduli of single-walled carbon nanotube ropes. Physical Review Letters 82, 944–947.

Sánchez-Portal, D., Artacho, E., Soler, J.M., 1999. Ab initio structural, elastic, and vibrational properties of carbon nanotubes. Physical Review B 59, 12678–12688.

Shenoy, V.B., Miller, R., Tadmor, E.B., Phillips, R., Ortiz, M., 1998. Quasicontinuum models of interfacial structure and deformation. Physical Review Letters 80, 742–745.

Shenoy, V.B., Miller, R., Tadmore, E.B., Rodney, D., Phillips, R., Ortiz, M., 1999. An adaptive finite element approach to atomic-scale mechanics—the quasicontinuum method. Journal of the Mechanics and Physics of Solids 47, 611–642.

Srivastava, D., Menon, M., Cho, K., 2001. Computational nanotechnology with carbon nanotubes and fullerenes. Computing in Science and Engineering 3 (4), 42–55.

Tadmor, E.B., Ortiz, M., Phillips, R., 1996a. Quasicontinuum analysis of defects in solids. Philosophy Magazin A 73, 1529–1563.

Tadmor, E.B., Phillips, R., Ortiz, M., 1996b. Mixed atomistic and continuum models of deformation in solids. Langmuir 12, 4529–4534.

Tersoff, J., 1988. New empirical approach for the structure and energy of covalent systems. Physical Review B 37, 6991–7000.

Thess, A., Lee, R., Nikolaev, P., Dai, H.J., Petit, P., Robert, J., Xu, C.H., Lee, Y.H., Kim, S.G., Rinzler, A.G., Colbert, D.T., Scuseria, G.E., Tomanek, D., Fischer, J.E., Smalley, R.E., 1996. Crystalline ropes of metallic carbon nanotubes. Science 273, 483–487.

Tombler, T.W., Zhou, C., Kong, J., Dai, H., Liu, L., Jayanthi, C.S., Tang, M., Wu, S.Y., 2000. Reversible electromechanical characteristics of carbon nanotubes under local-probe manipulation. Nature 405, 769–772.

Treacy, M.M.J., Ebbesen, T.W., Gibson, J.M., 1996. Exceptionally high Young's modulus observed for individual carbon nanotubes. Nature 381, 678–680.

Vaccarini, L., Goze, C., Henrard, L., Hernández, E., Bernier, P., Rubio, A., 2000. Mechanical and electronic properties of carbon and boron-nitride nanotubes. Carbon 38, 1681–1690.

Van Lier, G., Van Alsenoy, C., Van Doren, V., Geerlings, P., 2000. Ab initio study of the elastic properties of single-walled carbon nanotubes and graphene. Chemical Physics Letters 326, 181–185.

Wagner, H.D., Lourie, O., Feldman, Y., Tenne, R., 1998. Stress-induced fragmentation of multiwall carbon nanotubes in a polymer matrix. Applied Physics Letters 72, 188–190.

Walters, D.A., Ericson, L.M., Casavant, M.J., Liu, J., Colbert, D.T., Smith, K.A., Smalley, R.E., 1999. Elastic strain of freely suspended single-wall carbon nanotube ropes. Applied Physics Letters 74, 3803–3805.

Wong, E.W., Sheehan, P.E., Lieber, C.M., 1997. Nanobeam mechanics: elasticity, strength, and toughness of nanorods and nanotubes. Science 277, 1971–1975.

Yakobson, B.I., Avouris, Ph., 2001. Mechanical properties of carbon nanotubes. In: Dresselhaus, M.S., Dresselhaus, G., Avouris, Ph. (Eds.), Topics in Applied Physics, Springer–Verlag, Heidelberg, Germany, Carbon Nanotubes, vol. 80, pp. 287–329.

Yakobson, B.I., Brabec, C.J., Bernholc, J., 1996. Nanomechanics of carbon tubes: Instabilities beyond linear response. Physical Review Letters 76, 2511–2514.

Yakobson, B.I., Campbell, M.P., Brabec, C.J., Bernholc, J., 1997. High strain rate fracture and C-chain unraveling in carbon nanotubes. Computational Materials Science 8, 341–348.

Yu, M.F., Files, B.S., Arepalli, S., Ruoff, R.S., 2000a. Tensile loading of ropes of single wall carbon nanotubes and their mechanical properties. Physical Review Letters 84, 5552–5555.

Yu, M.F., Lourie, O., Dyer, M.J., Moloni, K., Kelly, T.F., Ruoff, R.S., 2000b. Strength and breaking mechanism of multiwalled carbon nanotubes under tensile load. Science 287, 637–640.

Zhang, P., Huang, Y., Gao, H., Hwang, K.C., 2002a. Fracture nucleation in single-wall carbon nanotubes under tension: a continuum analysis incorporating interatomic potentials. Journal of Applied Mechanics, in press.

Zhang, P., Klein, P., Huang, Y., Gao, H., Wu, P.D., 2002b. Numerical simulation of cohesive fracture by the virtual-internal-bond model. Computer Modeling in Engineering and Science, in press.

Zhou, G., Duan, W., Gu, B., 2001. First-principles study on morphology and mechanical properties of single-walled carbon nanotube. Chemical Physics Letters 333, 344–349.